JACS
JOURNAL OF THE AMERICAN CHEMICAL SOCIETY

Article

pubs.acs.org/JACS

# Controlling the Ring Curvature, Solution Assembly, and Reactivity of Gigantic Molybdenum Blue Wheels

Weimin Xuan, Andrew J. Surman, Haralampos N. Miras, De-Liang Long, and Leroy Cronin*

WestCHEM, School of Chemistry, University of Glasgow, University Avenue, Glasgow, G12 8QQ, United Kingdom

Supporting Information

**ABSTRACT:** We describe the synthesis, structure, self-assembly, solution chemistry, and mass spectrometry of two new gigantic decameric molybdenum blue wheels, $\{Mo_{200}Ce_{12}\}$ (**1**) and $\{Mo_{100}Ce_6\}$ (**2**), by building block rearrangement of the tetradecameric $\{Mo_{154}\}$ framework archetype and control of the architecture's curvature in solution from the addition of Ce(III). The assembly of **1** and **2** could be directed accordingly by adjusting the ionic strength and acidity of the reaction mixture. Alternatively, the dimeric cluster $\{Mo_{200}Ce_{12}\}$ could be transformed directly to the monomeric species $\{Mo_{100}Ce_6\}$ upon addition of a potassium salt. ESI-ion mobility mass spectra were successfully obtained for both $\{Mo_{200}Ce_{12}\}$ and $\{Mo_{100}Ce_6\}$, which is the first report in molybdenum blue chemistry thereby confirming that the gigantic clusters are stable in solution and that ion mobility measurements can be used to characterize nanoscale inorganic molecules.

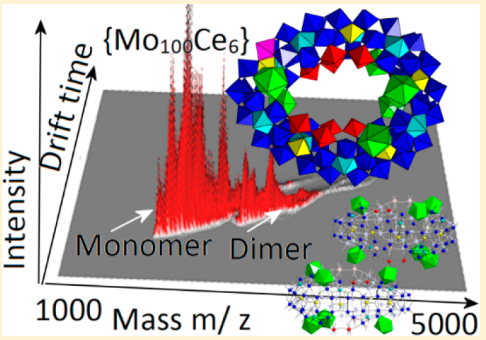


## INTRODUCTION

Polyoxometalates (POMs) are a class of molecular metal oxides of unmatched structural diversity, derived from assembly of large 'virtual combinatorial libraries' of building blocks.[1,2] Reflecting this structural diversity, POMs exhibit a wide range of properties, derived from the intrinsically redox-active and rigid anionic architectures, with myriad potential applications from medicine to catalysis and materials science.[3] One focus of this burgeoning field is the controlled fabrication of giant "nanosized" clusters, which bridge the gap between "traditional" molecular entities (<2 nm) and less precisely defined polymeric entities.[4] Such giant clusters have unique properties and can also be further incorporated into even larger assemblies or high-dimensional materials.[5] The past two decades have witnessed much growth in this area, facilitated by improvements in analytical and synthetic methodology, with the discovery of a number of these clusters with sizes in the 2−6 nm range.[6] Among the most well-researched species of this important family of giant POMs are the wheel-shaped $\{Mo_{154}\}$[2b] and $\{Mo_{176}\}$[6d] and the "hedgehog-like" $\{Mo_{368}\}$[5d] clusters whose size has helped define the concept of molecular nanotechnology. While the discovery of these clusters constitutes a great achievement, the rational design and assembly by deliberate manipulation of synthetic parameters are still in its infancy; indeed we still lack a basic understanding of how such vastly improbable structures are "selected" in solution from the myriad of combinatorial possibilities.[7a] As such, it remains a formidable task to design large POMs *de novo*, controlling the shape, functionality, and the cavities of the POM skeleton; as a result the structural and functional variety available in "giant" POMs remains limited.[4−7] Furthermore, molybdenum-blue-type clusters have not yet been directly and unambiguously observed by mass spectrometry, complicating the task of design by limiting their characterization almost exclusively to crystalline solids.

Polyoxometalate "big wheels" can be viewed as oligomeric assemblies of fundamental building blocks. In molybdenum blue (MB) wheels, the fundamental building blocks are based on $\{Mo(Mo)_5\}$ pentagons linked further by $\{Mo_2\}$ and $\{Mo_1\}$ units, typically producing a $\{Mo_8\}$ basic repeating building block,[7b,c] as illustrated in the archetypal tetradecameric $\{Mo_{154}\}$ and hexadecameric $\{Mo_{176}\}$. Considerable efforts have been made to develop new means to control the assembly of these building blocks, to produce new gigantic structures. To this end, novel decameric (e.g., $\{Mo_{96}La_8\}$[8a]) and dodecameric (e.g., $\{Mo_{120}Pr_6\}$,[8b] $\{Mo_{256}Eu_8\}$[8c]), species were produced by using strong electrophiles such as $La^{III}$, $Pr^{III}$, and $Eu^{III}$ ions to replace $\{Mo_2\} \equiv \{Mo^{VI}{}_2O_5(H_2O)_2\}^{2+}$ units on the parent isopolyoxomolybdate framework of $\{Mo_{154}\}$. The incorporation of lanthanide ions not only "breaks" the symmetry of $\{Mo_{154}\}$ on reorganization but also adjusts the curvature and functionalities of the inner surface.[8d,e] Despite all this work, it has not been possible to explore the assembly of such structures directly in solution or explore intermediate control of the ring curvature. This elusive information is crucial for further development and design of molecular nanosized materials with modular architectures (e.g., chirality)[8f] and functionalities.

Herein we report the synthesis of two novel lanthanide-doped MB wheels, $\{Mo_{200}Ce_{12}\}$ **1** $\{Mo_{100}Ce_6\}$ **2**, both based on a decameric skeleton. $Ce^{III}$ is used to modify the curvature of the ring. **1** and **2** were prepared by reducing an

**Received:** June 21, 2014
**Published:** September 4, 2014

   dx.doi.org/10.1021/ja5062483 | J. Am. Chem. Soc. 2014, 136, 14114−14120

acidified suspension of cerium polymolybdate in $H_2O$ and characterized by elemental analysis, single-crystal X-ray structure analysis, bond valence sum (BVS) calculations, thermogravimetry, IR, Raman, visible-NIR spectroscopy, and redox titrations. Also, the direct transformation of the dimeric **1** (Figure 1) to

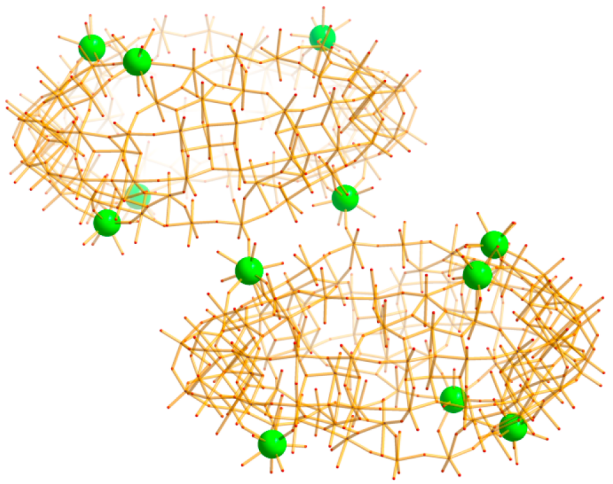

**Figure 1.** "Wire" representation of the dimer of **1a**. $Ce^{III}$ cations are highlighted as bright green spheres and Mo−O bonds as yellow wires.

monomeric **2** species observed by the addition of electrolyte. Compounds **1** and **2** can be formulated:

$$Ce_2^{III}(H_2O)_{18}K_2\{Mo_{80}^{VI}Mo_{20}^{V}Ce_6^{III}O_{306}H_{10}(H_2O)_{71}\}_2\cdot ca.400H_2O \equiv Ce_2(H_2O)_{18}K_2\{\mathbf{1a}\}_2\cdot ca.400H_2O \quad (1)$$

$$Ce^{III}(H_2O)_9K\{Mo_{80}^{VI}Mo_{20}^{V}Ce_6^{III}O_{306}H_{10}(H_2O)_{70}\}\cdot ca.140H_2O \equiv Ce(H_2O)_9K\{\mathbf{2a}\}\cdot ca.140H_2O \quad (2)$$

Furthermore, we report for the first time the Electrospray-Ionization Ion-Mobility-Mass Spectra (ESI-IMS-MS) of MB species (**1** and **2**), confirming their presence in solution and raising the possibility of higher-order assembly. Using this set of data we demonstrate the efficacy of the ESI-IMS-MS techniques as powerful tools for the investigation of the structure and chemistry of MB wheels in solution.

## EXPERIMENTAL SECTION

**Materials and Instrumentations.** All reagents and solvents were purchased from commercial sources and used as received. Elemental analyses (Mo, Ce, and K) were performed via ICP-OES. Thermogravimetric analysis was performed on a TA Instruments Q 500 thermogravimetric analyzer under nitrogen flow at a typical heating rate of 5 °C $min^{-1}$. UV−vis spectra were collected using a Shimadzu PharmaSpec UV-1700 UV−vis spectrophotometer in transmission mode using quartz cuvettes with 1.0 cm optical path length. Infrared spectra (4000−400 $cm^{-1}$) of all samples were recorded on JASCO FTIR-410 spectrometer or a JASCO FT-IR 4100 spectrometer. Raman spectra were collected on a Horiba Jobin-Yvon LabRAM-HR Raman microscope. The excitation wavelength was a 20 mW HeNe laser ($\lambda$ = 532.2 nm).

**Synthesis of Compound {$Mo_{200}Ce_{12}$} (1).** A solution of $CeCl_3\cdot 6H_2O$ (6.0 g, 16.4 mmol) in $H_2O$ (300 mL) was quickly added under stirring to an aqueous solution of $K_2MoO_4$ (5.9 g, 24.8 mmol) in $H_2O$ (300 mL). The yellow precipitate was collected by filtration after 30 min, washed with ice-cold $H_2O$, and dried at 120 °C for 5 h (yield: 7.2 g); IR (KBr; 1700−500 $cm^{-1}$): 1625 (m), 1384 (m), 937 (m), 859 (s), 761 (s), 699 $cm^{-1}$(m). To the solution of this precipitate 0.1 g), in a mixture of $H_2O$ (8 mL) and 1 M $HClO_4$ (0.8 mL), an aqueous solution (0.4 mL) of $[N_2H_4]\cdot 2HCl$ (10 g/L) was added. The solution was heated with medium stirring in a 50 mL Erlenmeyer flask (wide-necked; covered with a watch glass) at 80−85 °C for 1 h. The resulting deep-blue solution was then cooled to room temperature, filtered, and kept in a closed flask for 12 h. After a small amount of dark-blue precipitation was removed by filtration the filtrate was kept in an open 50 mL Erlenmeyer flask for 1 week. The deep-blue plate-like crystals were collected by filtration, washed with ice-cold $H_2O$, and dried under inert atmosphere over $CaCl_2$, yield: 15 mg (8.1% based on Mo). Characteristic IR bands (KBr; 1700−500 $cm^{-1}$): 1614 (m), 971 (m; $\nu$ (Mo═O)), 812 (s), 644 (s), 560 $cm^{-1}$ (s). Elemental analysis, calcd: K 0.49, Ce 4.77, Mo 47.86%; Found K 0.50, Ce 4.42, Mo 48.00%. [The calculated values are based on the partially hydrated structure (340 $H_2O$ molecules) including three additional severely disordered molecules of KCl found in the solvent area of the crystal structure's diffraction pattern.]

**Synthesis of Compound {$Mo_{100}Ce_6$} (2).** **2** was synthesized in a similar fashion as compound **1**. After the small amount of dark blue precipitation was removed by filtration, KCl (22 mg, 0.3 mmol) was added to the filtrate of **1.** Dark blue block-like crystals of **2** appeared after 1 day, collected by filtration, washed with ice-cold $H_2O$, and dried under inert atmosphere over $CaCl_2$, yield: 12 mg (6.2% based on Mo). Alternatively, **2** could also been synthesized by addition of acetic acid (20 mg) or 12-molybdophosphoric acid (20 mg) instead of KCl. Characteristic IR bands (KBr; 1700−500 $cm^{-1}$): 1620 (m), 971 (m; $\nu$ (Mo═O)), 906 (m), 796 (m), 640 (m), 558 $cm^{-1}$ (s). Elemental analysis, calcd: K 0.79, Ce 4.98, Mo 48.73%; found K 0.85, Ce 4.60, Mo 48.1%. [The calculated values are based on the hydrated structure (140 $H_2O$ molecules) including three additional severely disordered molecules of KCl existing (but not modelled) in the solvent area of the crystal structure.]

**X-ray Crystal Structure Analyses.** Suitable single crystal was selected and mounted onto a rubber loop using Fomblin oil. Single-crystal X-ray diffraction data of both **1** and **2** were recorded on a Bruker Apex CCD diffractometer ($\lambda$ ($MoK_\alpha$) = 0.71073 Å) at 150 K equipped with a graphite monochromator. Structure solution and refinement were carried out with SHELXS-97[9] and SHELXL-97[10] via WinGX.[11] Data collection and reduction were performed using the Apex2 software package and structure solution, and refinement was carried out by SHELXS-97[9] and SHELXL-97[10] using WinGX.[11] Corrections for incident and diffracted beam absorption effects were applied using empirical absorption correction. All the Mo atoms (including those disordered) and most of the O atoms were refined anisotropically. Potassium and cerium ions (inside the cavity of the ring) were identified and refined isotropically. Solvent water molecule sites with partial occupancy were found and included in the structure refinement. Crystallographic formulas typically contain much more water molecules in the crystal lattice than the formulas used for chemical analyses as the sample was dried up. It is important to note that with these structures we are moving outside the realm of small molecule crystallography and are dealing with refinements and problems that lie between small molecule and protein crystallography. As a result we cannot expect refinements and statistics to follow the path of crystals with much smaller unit cells. However, the final refinement statistics are relatively good, and in all cases the structural analysis allows us to unambiguously fully determine the structures of the compounds. Both structures of compounds **1** and **2** were deposited at ICSD, http://www.fiz-karlsruhe.de/icsd.html, with the numbers 427968 and 427969, respectively.

**ESI-IMS-MS Spectroscopy.** Samples were prepared by dissolving pure crystals of **1** and **2** in HPLC grade water, at approximately 5 mg/mL; these solutions were filtered (some solid always remained) and analyzed with no further purification. Spectra were acquired on a Waters Synapt G2 HDMS instrument in Sensitivity mode (except where otherwise stated), with samples infused into the standard ESI source at 5 $\mu$L/min using a Harvard syringe pump.

The following parameters were used for acquisition of all spectra (unless otherwise stated): ESI capillary voltage, 2.7 kV; sample cone voltage, 35 V; extraction cone voltage, 4.0 V; source temperature, 80 °C; desolvation temperature, 180 °C; cone gas ($N_2$) flow, 15 L/h; desolvation gas ($N_2$) flow, 750 L/h; source gas flow, 0 mL/min; trap gas flow,


dx.doi.org/10.1021/ja5062483 | J. Am. Chem. Soc. 2014, 136, 14114−14120

2 mL/min; helium cell gas flow, 180 mL/min; IMS gas flow, 90 mL/min; IMS DC entrance, 25.0; helium cell DC, 35.0; helium exit, −5; IMS bias, 3.0; IMS DC exit, 0; IMS wave velocity, 1000 m/s; IMS wave height, 40 V. Data were acquired using MassLynx v4.1 and initially processed using DriftScope v2.2. IMS-MS spectra are displayed with a linear intensity scale using the color-coding shown in the accompanying key; no filtering is applied to limit signals (e.g., no filtering of signals <5% in 2D map; that is, few other signals are visible in the raw data with no manipulation). To determine drift times ($t_D$) of species of interest in the IMS cell arrival time distribution (ATD), data were extracted from Driftscope/Masslynx, and fit to Gaussian curves using Fityk v0.9.8 to determine a representative retention times peak center.

Ion mobility calibration data were recorded for equine cytochrome C, oligothymidine,[12] and a another DNA strand (d[TTTAGGG]$_6$)[13] and fit to their respective helium collision cross sections ($CCS_{He}$) reported in the literature using the approach outlined in ref 14; data were only omitted where peaks were very weak, fitting not possible/ambiguous, or conformations not observed. The resulting calibration curve (see SI) was then used to estimate the $CCS_{He}$ of ions of interest from observed drift times.

## RESULTS AND DISCUSSION

**Synthesis of 1 and Transformation of Dimeric Species 1 to Monomeric 2.** **1** was prepared after the controlled reduction of a $Ce_2O_3{\cdot}7MoO_3$ suspension at low pH in aqueous solution upon heating. The filtered deep-blue mother liquor was left undisturbed for a week during which crystals of **1** were formed in moderate yield. **2** is the monomeric counterpart of **1** and discovered as a minor product during the synthesis of **1** (Figure 2). After optimization of the synthetic parameters, **2** could be easily obtained as the exclusive product by adding KCl to the mother liquor of **1**. Alternatively, **2** could also be produced by addition of acetic acid or 12-molybdophosphoric acid instead of KCl. The increase of ionic strength seems to promote the transformation of **1** to **2** while the increase of acidity the exclusive isolation of **2**.

**Structural Features of the Gigantic Wheels 1 and 2.** Single crystal X-ray structure analysis of **1** revealed a dimeric nanoring **1** structure, composed of two interconnected **2a** clusters via two $Ce^{III}$ cations. The dimers pack parallel to the crystallographic *ac* plane giving rise to 1D channels occupied by aquated $Ce^{III}$ ions and guest water molecules (Figure 3). The framework of **1a** is constructed by three basic "virtual" building blocks {$Mo_8$}, {$Mo_2$}, and {$Mo_1$}, previously observed in MB wheels (Figure 2) and thus is structurally related to the tetradecameric {$Mo_{154}$}[2b] and dodecameric archetypes {$Mo_{120}Pr_6$}[8b] and {$Mo_{256}Eu_8$},[8c] (Figure 2). The archetypal ring {$Mo_{154}$} consists of 14 sets of the three different building block types: {$Mo_8$}, {$Mo_1$}, and {$Mo_2$}, whereas the {$Mo_{100}Ce_6$} wheel presented here contains 10 {$Mo_8$} units, 4 {$Mo_2$} units, 10 {$Mo_1$} units, 2 {$Mo^*_1$} units, 4 {$Ce(H_2O)_5$} units, and 2 {$Ce(H_2O)_6$} units. The two new {$Mo_1$*} building units are located on the opposite side of two {$Ce(H_2O)_6$} (Figure S6).

The asymmetric arrangement of 6 $Ce^{3+}$ ions on the upper and lower surfaces of {$Mo_{100}Ce_6$} as well as the incorporation of two {$Mo^*_1$} fragments greatly reduce the symmetry of the wheel in **1a** and **2a** to $C_2$ as compared with parent {$Mo_{154}$} ($D_{7d}$ point group). Therefore, the wheel displays a relatively anisotropic structure with the ring to ring diameter compressed, featuring an irregular oval-shaped opening with outer and inner ring diameter of about 31 and 12 Å, respectively, at its most elongated points. Accordingly, the structure evolves from an almost ideal circular {$Mo_{154}$} to a severely distorted ellipse **1a**.

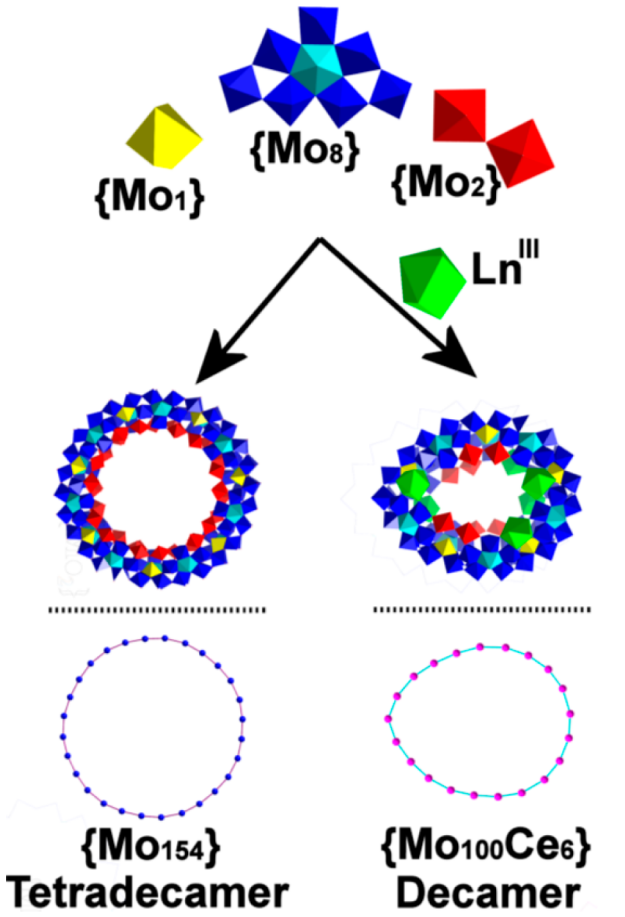


**Figure 2.** Top: Representation of the "virtual" building blocks leading to the synthesis of the parent {$Mo_{154}$} wheel or anion **2a** in the presence of $Ln^{III}$ cations (Middle). Bottom: Representation of the wheel's curvatures. Polyhedra have the Mo ions at the center, and oxygen ligands at the apexes are colored according to the accepted building blocks for these structures.[6−8]

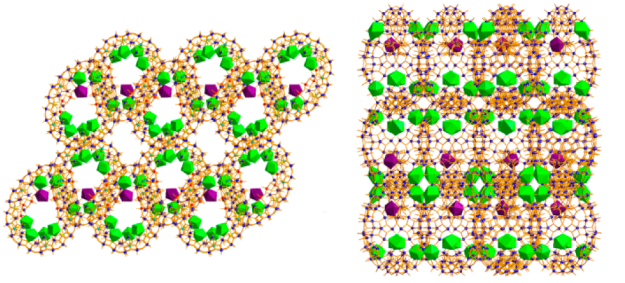

**Figure 3.** Representation of the packing diagram of **1** (left) and **2** (right) (along *b* axis. Aquated $Ce^{3+}$ ions within the channels are highlighted in purple, while $Ce^{3+}$ ions ligated to the wheels are colored green).

A further characteristic of the structure of the anion **1a** is the large number of protons resulting from the 20 $e^-$ reduction. The overall reduction state of the wheel was confirmed using three independent techniques (UV−vis spectroscopy, redox titration, and bond valence sum analysis). A careful analysis of the bond valence sums reveals 10 singly and 71 doubly protonated oxygen atoms. Singly protonated are the 10 equiv O atoms situated in the equatorial plane and linking two neighboring {$Mo_8$} units as well as another Mo atom that also lies in this plane.


dx.doi.org/10.1021/ja5062483 | J. Am. Chem. Soc. 2014, 136, 14114−14120

BVS calculations[15] are carried out on all the Mo and O centers (Table S4).[7a,8b,c] Taking into consideration the obtained information from the above calculations along with elemental analyses and redox titration, it is possible to determine the overall building-block scheme and overall charge for the **1a** as $[\{Mo_2\}_4\{Mo_1\}_{10}\{Mo_8\}_{10}\{Mo_1{*}\}_2\{Ce(H_2O)_5\}_4\{Ce(H_2O)_6\}_2] \equiv [\{Mo^{VI}{}_2O_5(H_2O)_2\}_4\{Mo^{VI/V}{}_8O_{26}(\mu\text{-}O)_2H(H_2O)_3Mo^{VI/V}\}_{10}\{Ce^{III}(H_2O)_5\}_4\{Ce^{III}(H_2O)_6\}_2\{Mo^{VI/V}O_3{*}\}_2]^{4-}$. In a similar fashion, single-crystal X-ray structure analysis revealed that **2** crystallizes in *Ibca* space group with **2a** as the core anion, which exhibits an identical ring shaped structure to the rings observed in **1a**. **2** displays a much more ordered and condensed packing mode than **1** (*P*-1) (Figure 3). Also, the BVS calculations and redox titrations for **2** gave similar values to those for **1** (Table S4), suggesting they have the same decameric anionic core containing 20 $Mo^V$ and 10 $\mu_3$-OH ions.

In total there are six $Ce^{III}$ ions coordinated on the wheel. More specifically, three ions are located on both upper and lower rim of the wheel. For each rim, two $Ce^{III}$ ions are adjacent at one end with the other at the opposite end; through this ion the two clusters **2a** are linked together via Mo−O−Ce (Mo−O, 1.7188(1) Å; Ce−O, 2.5671(1) Å) bonds to form the dimeric **1a**, with one ring superposing on another in an antiparallel orientation (Figure 1). The coordination configuration of the two distinct types of $Ce^{III}$ can be described as distorted monocapped square antiprism, built either from four $\mu_2$-O atoms and five $H_2O$ molecules or from three $\mu_2$-O atoms and six $H_2O$ molecules $-\{Ce(H_2O)_5\}$ and $\{Ce(H_2O)_6\}$, respectively, Figure 4. Finally, there is an additional aquated

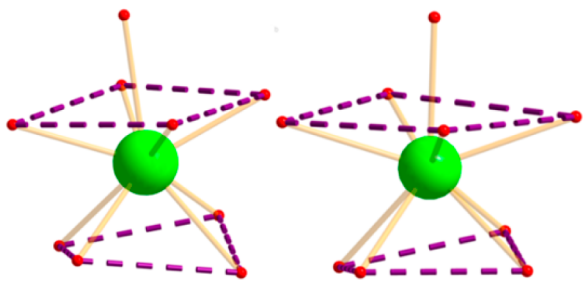

**Figure 4.** Representation of the coordination geometry of cerium cations, $\{Ce(H_2O)_5\}$ and $\{Ce(H_2O)_6\}$, emphasizing the distorted monocapped square antiprism coordination sphere.

cerium cation, $\{Ce(H_2O)_9\}$, "trapped" within the cavity of each wheel (highlighted purple in Figure 3).

Our reasoning for the incorporation of the more electrophilic $Ce^{III}$ ion was not only to alter the charge of the cluster but also to exert an influence on the curvature (and hence shape and size) of ring, as the $\{Ce(H_2O)_5\}$ and $\{Ce(H_2O)_6\}$ moieties are significantly smaller than the $\{Mo_2\}$ unit. Here we see that the two different substitution modes have tremendously distinct effects on the configuration of **1a** and consequently of **2a**. As shown in Figure 5, $\{Ce(H_2O)_5\}$ joins two sets of $\{Mo_8\}$ with four Mo−O−Ce bonds, in a manner similar to an $\{Mo_2\}$ unit. The six-membered $Mo_6$ ring, formed by one $\{Mo_2\}$ unit and four Mo atoms from two neighboring $\{Mo_8\}$ fragments in the parent cluster $\{Mo_{154}\}$ (Figure 5a), now shrinks and transforms into a new five-membered $Mo_4Ce$ ring (Figure 5b).

As a result, the average Mo−Mo distance of the two neighboring pentagonal bipyramidal Mo centers separated by the $\{Ce(H_2O)_5\}$ unit becomes significantly shorter (11.4915 Å)

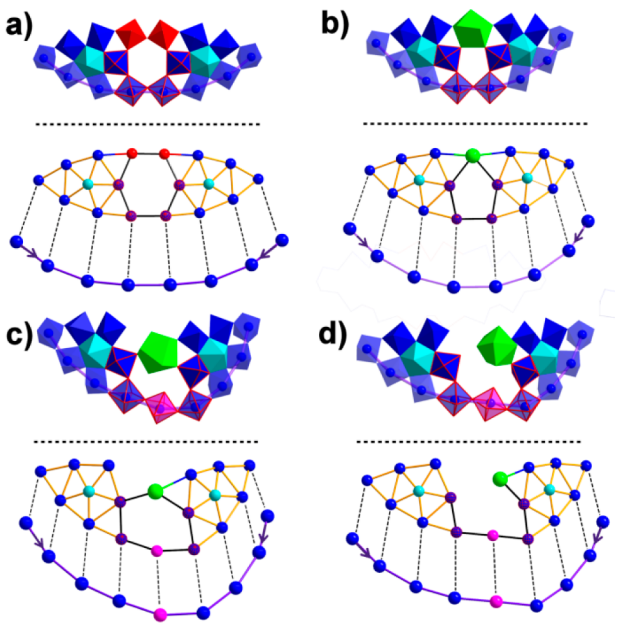


**Figure 5.** (a) Two $\{Mo_8\}$ units linked by one $\{Mo_2\}$ unit ($\{Mo2\}$, red; $\{Mo_8\}$, blue with central Mo in cyan; Mo atoms of $Mo_6$ ring are bordered in red; Mo atoms on the rim of $\{Mo_8\}$ units are presented in 50% transparency to highlight the purple bonds inserted between them). (b) Two $\{Mo_8\}$ units linked by one $\{Ce(H_2O)_5\}$ (Ce, green polyhedron). (c) Two $\{Mo_8\}$ units linked by one $\{Ce(H_2O)_6\}$ ($\{Mo_1{*}\}$, pink polyhedron). (d) Two $\{Mo_8\}$ units connected by one $\{Eu(H_2O)_7\}$ in the $\{Mo_{256}Eu_8\}$ wheel ($\{Mo_1{*}\}$, pink polyhedron).

comparing with the relevant one in the parent cluster (12.8960 Å). This considerably shorter distance is induced by the replacement of the $\{Mo_2\}$ by the $\{Ce(H_2O)_5\}$ unit, and this causes the contraction of the wheel and consequently increases the curvature of the ring. This is also supported by the altered trend in bond angles of Mo−Mo−Mo along the rim of $\{Mo_8\}$ units. As indicated by the purple line in Figure 5 (ball and stick representation), the corresponding angles show a continuous decrease from the two ends of $\{Mo_8\}$ units to the central $Mo_4Ce$ ring (from ∼164° to ∼158°) in contrast with gradual increase for the case of $\{Mo_2\}$ (from ∼161−164° to ∼171°) (Figure 5a,b and Table S3).

In a similar fashion on the opposite site on the ring's rim, the incorporation of the $\{Ce(H_2O)_6\}$ unit induces an average Mo−Mo separation of 12.43 Å, just slightly shorter than the distance observed in the parent cluster (12.89 Å). The reason is that the six-membered $Mo_5Ce$ ring (Figure 5c) is severely distorted comparing to the approximately coplanar $Mo_6$ or $Mo_4Ce$ (Figure 5a,b) ring due to the incorporation of an additional $\{Mo_1{*}\}$ unit between two $\{Mo_8\}$ fragments. This increases the size of $Mo_5Ce$ ring and provides more flexibility and space for two neighboring $\{Mo_8\}$ units to adjust and rearrange into a more favorable orientation (Figure 5c). Additionally, the two $\{Mo_8\}$ building blocks have to bend around the inserted $\{Mo_1{*}\}$ unit and adopt a twisted configuration in order to minimize the consequent tension. Correspondingly, the Mo−Mo−Mo angles experience a sharp decrease from ∼161−164° to 140° moving from the $\{Mo_8\}$ toward the central $\{Mo_1{*}\}$ unit (Table S3).

In an effort to compare the structural features of the new $\{Mo_{100}Ce_6\}$ ring (in **1a** and **2a**) and the previously reported Ln-containing MB wheels, $\{Mo_{120}Pr_6\}$[8b] and $\{Mo_{256}Eu_8\}$,[8c] we came across a noteworthy difference in relation to the


dx.doi.org/10.1021/ja5062483 | J. Am. Chem. Soc. 2014, 136, 14114−14120

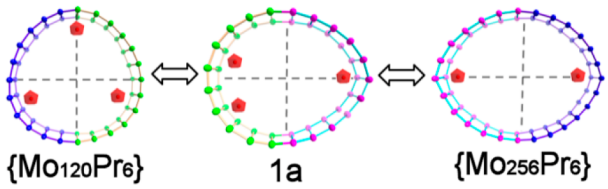


**Figure 6.** Schematic representation of $\{Mo_{120}Pr_6\}$, **1a** and $\{Mo_{256}Eu_8\}$ by connecting Mo atoms on the rim of equator of the wheels ($Ln^{3+}$ ions on the lower rim are highlighted in red polyhedra, the symmetry-related $Ln^{3+}$ ions on upper rim are omitted for clarity).

observed curvatures, see Figure 6. More specifically, the $Pr^{III}$ and $Eu^{III}$-doped rings exhibit more regular shapes. This is due to the even distribution of the six $\{Pr(H_2O)_5\}$ ions across the wheel's rim alternating with $\{Mo_2\}$ fragments in the $\{Mo_{120}Pr_6\}$ structure; whereas four $\{Eu(H_2O)_7\}$ ions occupy antipodal positions (Figure 6) in the case of $\{Mo_{256}Eu_8\}$. In our case, **1a** falls between the two symmetric distributions. Consequently, the aspect ratio (longest:shortest distance of the wheel's cavity) of the wheels increases progressively in a sequence from $\{Mo_{154}\}$ to $\{Mo_{120}Pr_6\}$, then to **1a** and $\{Mo_{256}Eu_8\}$ (Table 1),

**Table 1. Summary of the Building Blocks and Curvatures of {Mo154}, 1a, $\{Mo_{120}Pr_6\}$, and $\{Mo_{256}Eu_8\}$**

| compounds | building blocks | aspect ratio |
|---|---|---|
| $\{Mo_{154}\}^{2b}$ | $\{Mo_1\}_{14}\{Mo_2\}_{14}\{Mo_8\}_{14}$ | 1.01 |
| $\{Mo_{120}Pr_6\}^{8b}$ | $\{Mo_1\}_{12}\{Mo_2\}_6\{Mo_8\}_{12}$ $\{Pr(H_2O)_5\}_6$ | 1.06 |
| **1a** | $\{Mo_1\}_{10}\{Mo_2\}_4\{Mo_8\}_{10}$ $\{Mo_1{*}\}_2\{Ce(H_2O)_5\}_4\{Ce(H_2O)_6\}_2$ | 1.23 |
| $\{Mo_{256}Eu_8\}^{8c}$ | $\{Mo1\}_{12}\{Mo_2\}_8\{Mo_8\}_{12}$ $\{Mo_1{*}\}_4\{Eu(H_2O)_7\}_4$ | 1.33 |

showing how the ring curvature can be controlled by the addition of lanthanide ions.

**ESI-IMS-MS Spectroscopic Study of Solutions of 1 and 2.** Electrospray mass spectrometry (ESI-MS) has proved invaluable in understanding the formation and behavior of POM clusters, and for our efforts to shift from their discovery to their design,[16] however, thus far ESI-MS of the giant MB clusters has proved elusive. To further characterize **1** and investigate the availability of the wheel **1a** in solution for higher order assembly, we attempted electrospray-ion mobility mass spectrometry (ESI-IMS-MS) analysis of aqueous solutions made from dissolving crystals of **1.**

Viewed without ion mobility data, the ESI-MS spectrum consists of a series of broad peak envelopes (see upper trace in Figure 7). Alone this might represent weak evidence of intact rings, however separation in the IMS drift tube (the second dimension in the main 2D rendering in Figure 7) makes it clear that one main rigid size/shape dominates. While the peak envelopes are broad due to association of a range of counterions and solvent molecules (typical in ESI-MS of larger POMs),[17] the maxima in a series of charge states are consistent in mass, charge, and collision cross-section (CCS, *vide infra*) with intact wheel **1a** becoming charged through the loss of $Ce^{3+}$.

Further, a series of distribution envelopes corresponding to a larger structure is observable, consistent with a dimer/aggregate of two such wheels. These "dimeric" species are absent in the corresponding ESI-IMS-MS of solutions of **2**, which lacks the dimer. It is not possible to determine by MS alone whether this

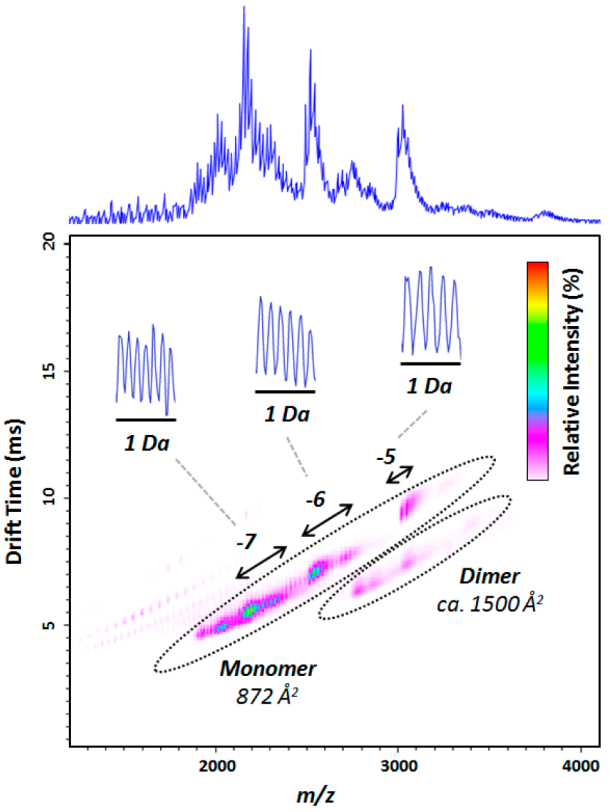


**Figure 7.** ESI-IMS-MS of an aqueous solution of **1**. Relative intensity (cf. highest peak) is shown on a linear scale (using the colored scale, inset); samples of isotope patterns (inset) were obtained in Resolution mode; see SI for details.

shows the dimer to be present in solution or formed on transfer to the gas phase (discussion in SI). Nonetheless, the difference between the spectra of **1** and **2** is striking and highlights the potential of ESI-IMS-MS as a tool to reveal the solution chemistry of POMs similar to other inorganic assemblies (Table 2).[18]

**Table 2. Data and Putative Assignment for Major Peaks in ESI-IMS-MS Spectrum of 1**

| $m/z_{Obs}$ | $z$ | $t_D$ (ms) | $CCS_{He}$ (Å$^2$) | assignment | $m/z_{Cal}$ |
|---|---|---|---|---|---|
| 2169 | −7 | 5.43 | 851 | $Mo_{100}Ce_5O_{305}H_8$ | 2168.8 |
| 2533 | −6 | 7.32 | 887 | $Mo_{100}Ce_5O_{306}H_{11}$ | 2533.4 |
| 3041 | −5 | 9.54 | 878 | $Mo_{100}Ce_5O_{306}H_{12}$ | 3040.3 |

In the study of other classes of structures, such as proteins, ESI-IMS-MS is used to measure the CCS of species of interest. This can be seen as representing size and shape and is valuable to quantify as it can then be compared to CCS values modeled for different putative structures, inferring the structure in the gas phase, and in solution.[19] As far to our knowledge this is the first report of ESI-MS and ESI-IMS-MS studies and calculation of the relevant CCS values for MB species. Using commercial instruments, $CCS_{He}$ is estimated using a calibration curve of similarly sized species of known $CCS_{He}$; this yielded an estimate of 872 Å$^2$ for the dominant "monomer" structure, and a rough value of around 1500 Å$^2$ for the weak putative dimer peaks (large POMs vary little in size between charge states,[17] so averages are representative). Modeling of the $CCS_{He}$ of **1a** (using a standard CCS modeling procedure, see SI for details


dx.doi.org/10.1021/ja5062483 | J. Am. Chem. Soc. 2014, 136, 14114−14120

and discussion) produces values similar to the experimentally determined $CCS_{He}$ (e.g., TM method gives $CCS_{Calc}$ of ca. 820 Å$^2$): remarkably close, considering that the parameter set used was validated mainly with proteins and carbon nanostructures. While this approach clearly requires some validation before POM structures can confidently be inferred, and the discrepancy between modeled and measured values reflects the need for a more appropriate parameter set to model metal oxide structures, this first investigation suggests great promise for the study of giant POMs.

## ■ CONCLUSIONS

In summary, two novel decameric clusters **1** and **2** have been successfully constructed using cerium ions, allowing control of wheel's curvature and reactivity. The synthesis could be easily controlled by addition of potassium ions after reaction, allowing **2** or **1** to be selected. This is the first report of both selective synthesis of a MB monomer/dimer set and transformation between the two. This controlled approach to synthesis of gigantic POMs incorporating "active sites" in their anionic scaffolds promises their availability as "molecular synthons" for higher-order assembly. Furthermore, ESI-IMS-MS confirms these "synthons" to be intact and available in solution (with very few other species observable) and to the best of our knowledge represents the first reported mass spectra of MB species, and one of the first ion mobility studies of large inorganic species. This finding is fundamentally important which goes beyond the MB family, as very few methods exist to confirm unambiguously solution behavior and structure of large metal oxide species. In future work we will attempt to use a combination of solution techniques to both map and control the assembly of gigantic MB structures in solution as well as looking to construct even larger systems aiming to exceed 10 nm in size for a single molecule.

## ■ ASSOCIATED CONTENT

### Ⓢ Supporting Information

Experimental details, characterization data, and crystallographic parameters (CIF). This material is available free of charge via the Internet at http://pubs.acs.org.

## ■ AUTHOR INFORMATION

### Corresponding Author

lee.cronin@glasgow.ac.uk

### Notes

The authors declare no competing financial interest.

## ■ ACKNOWLEDGMENTS

We thank Prof. Paul Kögerler (RWTH Aachen) for elemental analysis. We thank the EPSRC and the University of Glasgow for funding. L.C. thanks the Royal Society/Wolfson Foundation for a Merit Award.

## ■ REFERENCES

(1) (a) Special Issue on Polyoxometalates, *Chem. Rev.* **1998**, *98*, 1−390. (b) Pope, M. T.; Müller, A. *Polyoxometalate Chemistry: From Topology via Self-Assembly to Applications*; Kluwer: Dordrecht, 2001. (c) Long, D.-L.; Tsunashima, R.; Cronin, L. *Angew. Chem., Int. Ed.* **2010**, *49*, 1736−1758. (d) Miras, H. N.; Yan, J.; Long, D.-L.; Cronin, L. *Chem. Soc. Rev.* **2012**, *41*, 7403−7430. (e) Cadot, E.; Sokolov, M. N.; Fedin, V. P.; Simonnet-Jégat, C.; Floquet, S.; Sécheresse, F. *Chem. Soc. Rev.* **2012**, *41*, 7335−7353.

(2) (a) Müller, A.; Krickemeyer, E.; Bögge, H.; Schmidtmann, M.; Peters, F. *Angew. Chem., Int. Ed.* **1998**, *37*, 3359−3363. (b) Müller, A.; Krickemeyer, E.; Meyer, J.; Bögge, H.; Peters, F.; Plass, W.; Diemann, E.; Dillinger, S.; Nommenbruch, F.; Randerath, M.; Menke, C. *Angew. Chem., Int. Ed.* **1995**, *34*, 2122−2123. (c) Yan, J.; Gao, J.; Long, D.-L.; Miras, H. N.; Cronin, L. *J. Am. Chem. Soc.* **2010**, *132*, 11410−11411. (d) Zang, H.-Y.; Miras, H. N.; Long, D.-L.; Rausch, B.; Cronin, L. *Angew. Chem., Int. Ed.* **2013**, *52*, 6903−6906. (e) Ismail, A. H.; Bassil, B. S.; Yassin, G. H.; Keita, B.; Kortz, U. *Chem.—Eur. J.* **2012**, *18*, 6163−6166.

(3) (a) Dolbecq, A.; Dumas, E.; Mayer, C. R.; Mialane, P. *Chem. Rev.* **2010**, *110*, 6009−6048. (b) Hasenknopf, B. *Front. Biosci.* **2005**, *10*, 275. (c) Polyoxometalates in catalysis: Hill, C. L. *J. Mol. Catal. A: Chem.* **2007**, *262*, 1−242. (d) Noro, S.-i.; Tsunashima, R.; Kamiya, Y.; Uemura, K.; Kita, H.; Cronin, L.; Akutagawa, T.; Nakamura, T. *Angew. Chem., Int. Ed.* **2009**, *48*, 8703−8706. (e) Liu, T.; Diemann, E.; Li, H.; Dress, A. W. M.; Müller, A. *Nature* **2003**, *426*, 59−62.

(4) (a) Müller, A.; Gouzerh, P. *Chem. Soc. Rev.* **2012**, *41*, 7431−7463. (b) Gouzerh, P.; Che, M. *Actual. Chim.* **2006**, 9−22. (c) Banerjee, A.; Bassil, B. S.; Röschenthaler, G.-V.; Kortz, U. *Chem. Soc. Rev.* **2012**, *41*, 7590−7604. (d) Song, Y.-F.; Tsunashima, R. *Chem. Soc. Rev.* **2012**, *41*, 7384−7402. (e) Proust, A.; Matt, B.; Villanneau, R.; Guillemot, G.; Gouzerh, P.; Izzet, G. *Chem. Soc. Rev.* **2012**, *41*, 7605−7622.

(5) (a) Müller, A.; Krickemeyer, E.; Bögge, H.; Schmidtmann, M.; Peters, F.; Menke, C.; Meyer, J. *Angew. Chem., Int. Ed.* **1997**, *36*, 483−486. (b) Müller, A.; Das, S. K.; Bögge, H.; Beugholt, C.; Schmidtmann, M. *Chem. Commun.* **1999**, 1035−1036. (c) Mitchell, S. G.; Streb, C.; Miras, H. N.; Boyd, T.; Long, D.-L.; Cronin, L. *Nat. Chem.* **2010**, *2*, 308−312. (d) Müller, A.; Beckmann, E.; Bögge, H.; Schmidtmann, M.; Dress, A. *Angew. Chem., Int. Ed.* **2002**, *41*, 1162−1166.

(6) (a) de La Oliva, A. R.; Sans, V.; Miras, H. N.; Yan, J.; Zang, H.-Y.; Richmond, C. J.; Long, D.-L.; Cronin, L. *Angew. Chem., Int. Ed.* **2012**, *51*, 12759−12762. (b) Fang, X.; Kögerler, P.; Furukawa, Y.; Speldrich, M.; Luban, M. *Angew. Chem., Int. Ed.* **2011**, *50*, 5212−5216. (c) Müller, A.; Krickemeyer, E.; Bögge, H.; Schmidtmann, M.; Beugholt, C.; Kögerler, P.; Lu, C. *Angew. Chem., Int. Ed.* **1998**, *37*, 1220−1223. (d) Müller, A.; Shah, S. Q. N.; Bögge, H.; Schmidtmann, M. *Nature* **1999**, *397*, 48−50. (e) Botar, B.; Kögerler, P.; Hill, C. L. *J. Am. Chem. Soc.* **2006**, *128*, 5336−5337. (f) Izarova, N. V.; Kondinski, A.; Vankova, N.; Heine, T.; Jäger, P.; Schinle, F.; Hampe, O.; Kortz, U. *Chem.—Eur. J.* **2014**, *20*, 8556−8560. (g) Miras, H. N.; Cooper, G. J. T.; Long, D.-L.; Bögge, H.; Müller, A.; Streb, C.; Cronin, L. *Science* **2010**, *327*, 72−74. (i) Miras, H. N.; Richmond, C. J.; Long, D.-L.; Cronin, L. *J. Am. Chem. Soc.* **2012**, *134*, 3816−3824.

(7) (a) Scullion, R. A.; Surman, A. J.; Xu, F.; Mathieson, J. S.; Long, D.-L.; Haso, F.; Liu, T.; Cronin, L.; *Angew. Chem., Int. Ed.*, **2014**, in press, DOI: 10.1002/anie.201404621. (b) Müller, A.; Serain, C. *Acc. Chem. Res.* **2000**, *33*, 2−10. (c) Müller, A.; Roy, S. *Coord. Chem. Rev.* **2003**, *245*, 153−166.

(8) (a) Yamase, T.; Kumagai, S.; Prokop, P. V.; Ishikawa, E.; Tomsa, A.-R. *Inorg. Chem.* **2010**, *49*, 9426−9437. (b) Müller, A.; Beugholt, C.; Bögge, H.; Schmidtmann, M. *Inorg. Chem.* **2000**, *39*, 3112−3113. (c) Cronin, L.; Beugholt, C.; Krickemeyer, E.; Schmidtmann, M.; Bögge, H.; Kögerler, P.; Luong, T. K. K.; Müller, A. *Angew. Chem., Int. Ed.* **2002**, *41*, 2805−2808. (d) Yamase, T.; Ishikawa, E.; Abe, Y.; Yano, Y. *J. Alloys Compd.* **2006**, *408−412*, 693−700. (e) Ishikawa, E.; Yano, Y.; Yamase, T. *Materials* **2010**, *3*, 64−75. (f) Seliverstov, A.; Streb, C. *Chem. Commun.* **2014**, *50*, 1827−1829.

(9) Sheldrick, G. *Acta Crystallogr., Sect A* **1990**, *46*, 467−473.

(10) Sheldrick, G. *Acta Crystallogr., Sect A* **2008**, *64*, 112−122.

(11) Farrugia, L. *J. Appl. Crystallogr.* **1999**, *32*, 837−838.

(12) Hoaglund, C. S.; Liu, Y.; Ellington, A. D.; Pagel, M.; Clemmer, D. E. *J. Am. Chem. Soc.* **1997**, *119*, 9051−9052.

(13) Baker, E. S.; Bernstein, S. L.; Gabelica, V.; De Pauw, E.; Bowers, M. T. *Int. J. Mass Spectrom.* **2006**, *253*, 225−237.

(14) Smith, D. P.; Knapman, T. W.; Campuzano, I.; Malham, R. W.; Berryman, J. T.; Radford, S. E.; Ashcroft, A. E. *Eur. J. Mass. Spectrom.* **2009**, *15*, 113−130.

(15) Brown, I. D. *In Structure and Bonding in Crystals*; O'Keeffe, M. Navrotsky, A., Eds; Academic Press: New York, 1981; Vol. *II*, pp 1−30.
(16) (a) Miras, H. N.; Wilson, E. F.; Cronin, L. *Chem. Commun.* **2009**, 1297−1311. (b) Wilson, E. F.; Miras, H. N.; Rosnes, M. H.; Cronin, L. *Angew. Chem., Int. Ed.* **2011**, *50*, 3720. (c) Miras, H. N.; Stone, D. J.; McInnes, E. J. L.; Raptis, R. G.; Baran, P.; Chilas, G. I.; Sigalas, M. P.; T. Kabanos, A.; Cronin, L. *Chem. Commun.* **2008**, 4703. (d) Yan, J.; Long, D.-L.; Miras, H. N.; Cronin, L. *Inorg. Chem.* **2010**, *49*, 1819−1825.
(17) (a) Robbins, P. J.; Surman, A. J.; Thiel, J.; Long, D.-L.; Cronin, L. *Chem. Commun.* **2013**, *49*, 1909−1911. (b) Miras, H. N.; Zang, H. Y.; Long, D.-L.; Cronin, L. *Eur. J. Inorg. Chem.* **2011**, 5105−5111.
(18) Brocker, E. R.; Anderson, S. E.; Northrop, B. H.; Stang, P. J.; Bowers, M. T. *J. Am. Chem. Soc.* **2010**, *132*, 13486−13494.
(19) Bernstein, S. L.; Wyttenbach, T.; Baumketner, A.; Shea, J. E.; Bitan, G.; Teplow, D. B.; Bowers, M. T. *J. Am. Chem. Soc.* **2005**, *127*, 2075−2084.